Capability of a novel impingement heat transfer device for application in future solar thermal receivers

Cite as: AIP Conference Proceedings **2303**, 030014 (2020); https://doi.org/10.1063/5.0029156
Published Online: 11 December 2020

Derwalt J. Erasmus, Matti Lubkoll, Ken J. Craig, and Theodor W. von Backström

Capability of a Novel Impingement Heat Transfer Device for Application in Future Solar Thermal Receivers

Derwalt J. Erasmus[1, a)], Matti Lubkoll[1], Ken J. Craig[2] and Theodor W. von Backström[1]

[1]*Solar Thermal Energy Research Group (STERG), Department of Mechanical and Mechatronic Engineering, Stellenbosch University, Private Bag X1, Matieland 7602, South Africa.*
[2]*Department of Mechanical and Aeronautical Engineering, University of Pretoria, Pretoria 0002, South Africa*

[a)]Corresponding author: erasmusderwalt@gmail.com

Abstract. CSP receivers are designed to permit higher outlet temperatures in order to enable higher theoretical efficiencies of the associated thermodynamic cycles. For pressurized air receivers, it is attempted to increase the operating temperature of metallic pre-heaters to then achieve high air outlet temperatures with cascaded ceramic receivers. Two limitations of metallic pressurized air receivers are cost and material creep at elevated temperatures and pressures. Therefore, it is necessary to maximize heat transfer from the receiver surface to the working fluid while minimizing the material surface temperature. Current research has demonstrated that jet impingement heat transfer devices are appropriate for application in thermal receivers because of the associated desirable heat transfer characteristics. However, it is shown that significant pressure losses are caused by such impinging jets because of the sudden expansion phenomenon. A novel enhanced impingement heat transfer device is presented in this paper. Experimental testing was conducted to investigate the domain comparatively with impinging jet configurations. The device is shown to be capable of delivering an enhanced surface heat transfer coefficient while affecting a lower total pressure loss around the domain when compared with similar impinging jet configurations. The geometry of the device can also be chosen to achieve a favorable combination of heat transfer and pressure loss characteristics. The device is applicable within the SCRAP concept and may be implementable within the SOLHYCO and SOLUGAS receivers. The device may also find an application in a parabolic dish collector. Finally, a novel receiver concept that incorporates the device in a tessellated structure is introduced – the SUNflower.

INTRODUCTION

Concentrating solar thermal energy can be used to supply heat to a Brayton thermodynamic cycle in order to generate electricity. A higher operating temperature of a thermodynamic cycle is associated with a higher theoretical thermal efficiency. Micro gas turbines operate at temperatures of around 1000 °C and axial flow gas turbines can operate at around 1500 °C. Metallic pressurized air receivers typically operate at temperatures above 800 °C. This is in order to pre-heat a pressurized air stream to this temperature and supply a cascaded combustor or alternatively a secondary ceramic receiver, which supplies the remainder of the heat for the downstream gas turbine. The operating temperature of metallic pressurized air receivers is near the creep strength material limits of high performance materials [1].

For this reason, it is necessary to maximize heat transfer from the receiver surface to the working fluid in order to reduce the material surface temperature. A large surface heat transfer coefficient is required within the device to achieve this. Impingement heat transfer finds potential applications in thermal receivers because of large achievable heat transfer coefficients. An impingement heat transfer device incorporates a high velocity fluid stream that impacts onto a surface, thereby transferring heat between the surface and the fluid. Current research involving such devices in receiver concepts include [2, 3, 4, 5, 6 & 7].

Because an impinging jet develops a large dynamic pressure, a significant total pressure loss may be observed. The consequential pressure loss adversely affects the performance of the thermodynamic cycle as shown in [5].

SolarPACES 2019
AIP Conf. Proc. 2303, 030014-1–030014-8; https://doi.org/10.1063/5.0029156
Published by AIP Publishing. 978-0-7354-4037-1/$30.00

For this reason, the heat transfer coefficient and the total pressure loss must be considered together when designing a suitable impingement heat transfer device.

A novel impingement heat transfer device that has been designed with these considerations will now be presented and investigated in this paper. The device is called the 'Tadpole'.

Introduction of the Tadpole Innovation

The Tadpole concept originated from an investigation of jet impingement heat transfer within a hemisphere [8] for application within the Spiky Central Receiver Air Pre-heater (SCRAP) concept [4]. In this domain, air enters through an inner tube, impinges onto the interior of a hemisphere and returns though an annulus. The Tadpole application within the SCRAP is presented in Figure 1. With the implementation of the Tadpole, the SCRAP concept may benefit from enhanced heat transfer characteristics and pressure recovery at the tip section of the spikes.

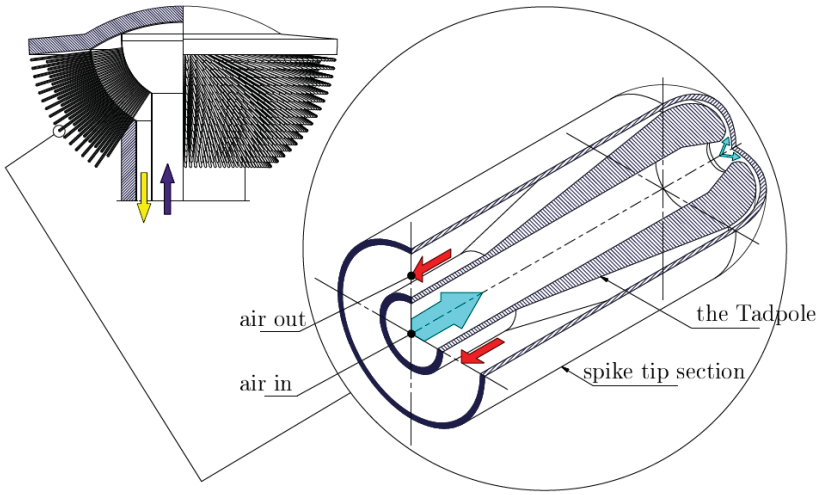

FIGURE 1: The implementation of a Tadpole manifestation on the SCRAP concept (adapted from [4])

The name, 'Tadpole', originates from the shape that is displaced in an axisymmetric flow domain – this is demonstrated in Figure 2. Figure 3 demonstrates a cross-sectional comparison of total pressure contoured path lines from a Reynolds Averaged Navier Stokes (RANS) Computational Fluid Dynamics (CFD) simulation between an impinging jet and a Tadpole manifestation.

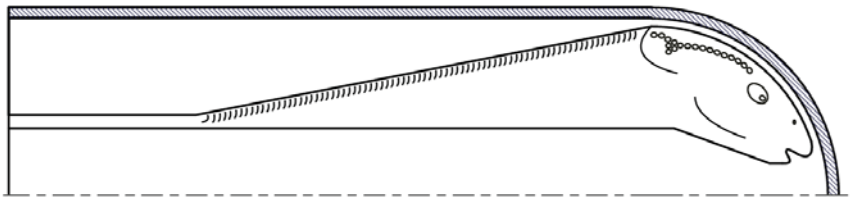

FIGURE 2: An axisymmetric illustration demonstrating the origin of the 'Tadpole'

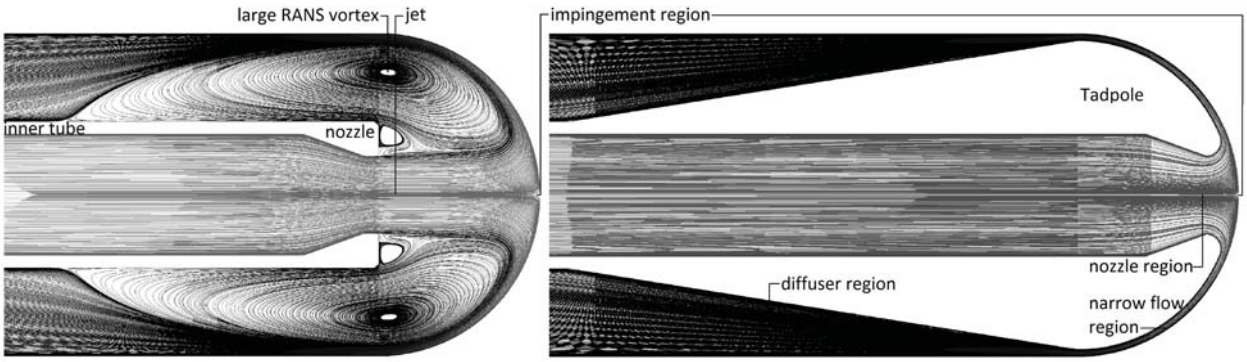

FIGURE 3: A cross-sectional comparison of RANS CFD total pressure contoured path lines between an impinging jet (left) and a Tadpole manifestation (right)

It was discovered that an impinging jet (shown on the left) develops a large dynamic pressure which is expanded with a sudden increase in flow area. The sudden expansion of the flow causes mechanical energy to be dissipated through viscous heating. In the domain of rapid expansion, large RANS ring vortices are characteristically observed.

The Tadpole was conceived with the idea of replacing the region containing ring vortices with a solid device – shown on the right of Fig. 3. It is shown that the implementation of the Tadpole decreases the change in total pressure. The Tadpole comprises a high velocity impingement heat transfer region, a high velocity narrow flow region and a diffuser to recover the generated dynamic pressure.

An illustration of the heat transfer occurring within the domain is given in Figure 4. It is shown that heat transfer occurs mainly near the impingement region and the narrow flow region as well as within the diffuser, to a lesser extent.

The heat transfer and pressure loss characteristics of a Tadpole prototype can be adjusted to achieve a favorable combination by modifying the relative axial distance between the hemispheres of the Tadpole and the heat transfer surface. Such an adjustment significantly affects the flow area development within the narrow flow region.

To understand the capabilities of the heat transfer device, an experimental investigation on the Tadpole's flow domain as well as on that of a normal impinging jet configuration will be presented – this will enable a performance comparison.

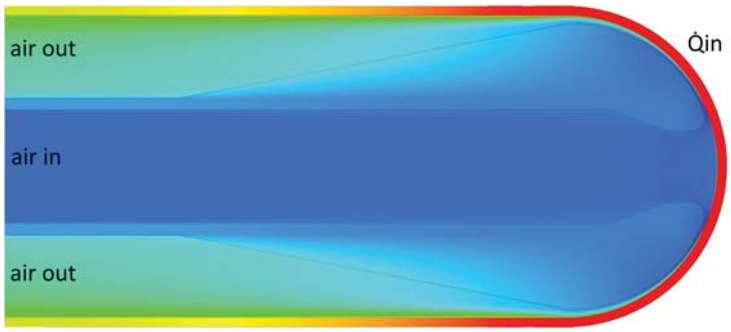

FIGURE 4: A cross-sectional illustration of RANS CFD temperature contours, demonstrating the heating of an air stream within the Tadpole's flow domain

EXPERIMENTAL TEST SETUP

The heat transfer and the consequential total pressure loss characteristics of the device are to be investigated. The experimental apparatus built by [9] was modified for this domain. The apparatus is presented in Figure 5.

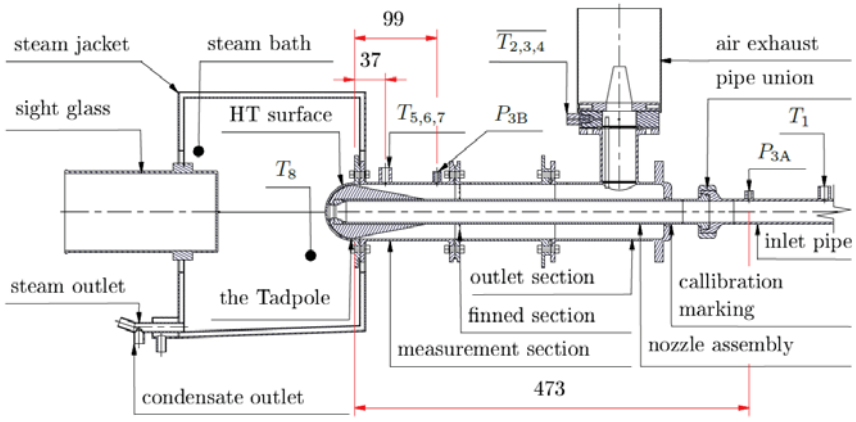

FIGURE 5: A sectional view of the significant components within the experimental apparatus (dimensions in mm)

The steam bath is filled with saturated steam at atmospheric pressure – nominally 100 °C – and provides heat for the apparatus. Steam condensation on the exterior 'HT surface' provides a near constant temperature boundary condition.

Pressurized air enters at the air inlet and travels through the nozzle assembly towards the Tadpole prototype. Heat is added to the air stream from the steam bath near the prototype. The air then travels through the measurement section towards an exhaust at the outlet which pressurizes the upstream flow domain. The mass flow rate of the air stream is controlled by varying the static pressure upstream of the inlet air between 0 bar – 8 bar.

The mass flow rate of the air and the total pressure at the air inlet and the measurement section are determined from a combination of differential pressure transducers and a gauge pressure sensor. Mass conservation and the ideal gas law are used to derive the results. The total pressure loss around the domain is calculated from the difference of both the static and dynamic pressures:

$$\Delta P_{\mathrm{t}} = (P_{\mathrm{s,3A}} + P_{\mathrm{d,3A}}) - (P_{\mathrm{s,3B}} + P_{\mathrm{d,3B}}). \tag{1}$$

Where 3A and 3B refer to the pressure tap positions at the inlet pipe and at the (downstream) measurement section, respectively — as shown in Fig. 5. The heat addition, $\dot{Q}_{\mathrm{air}}$, is determined using an energy balance between the air inlet and the air exhaust with temperature readings. These temperature readings are taken from thermocouples positioned at the air inlet (T_1) and at the air outlet (with an averaged reading of $T_{2,3,4}$). The interior 'HT surface' temperature, T_{is}, is derived using the steam saturation temperature (T_8) and a one dimensional condensation and conduction heat transfer thermal resistance network. This temperature is maintained near the steam saturation temperature. The interior surface heat transfer coefficient can now be calculated:

$$h_{\mathrm{is}} = \frac{\dot{Q}_{\mathrm{air}}}{A_{\mathrm{is}}(T_{\mathrm{is}} - T_1)}. \tag{2}$$

The experimental Tadpole prototypes have been 3-D printed from an ABS plastic compound. The remainder of the significant test section components are machined from aluminum. Aluminum was chosen because it is cost effective to machine and appropriate for investigating conjugate heat transfer at a relative low temperature.

The experimental apparatus was designed with the additional objective of validating a CFD model. The CFD model can be used to predict the thermal efficiency of the application concepts in further work.

Sensor Information, Calibration and Data Processing

Freescale MPX2050DP differential pressure transducers were used for measuring differential static pressure losses and were calibrated with a water manometer and a mercury manometer.
A First-rate FST800-10B gauge pressure sensor was used to determine the system static pressure and was calibrated using a reference pressure gauge. T-type thermocouples were used for temperature measurements and were calibrated using a FLUKE 9142 dry well calibrator. The experimental results are time averaged over 10 minutes after steady state heat transfer is reached and sensor measurements were taken at 4 second intervals.

Uncertainty

An uncertainty analysis was conducted to determine the mean and maximum uncertainty for the experimental results. The uncertainty calculations are based on [10]. The sensor reading deviations (after calibration) from calibration measurements form the basis of the error analysis. These deviations are used to predict an accumulated effect on the processed results to obtain an uncertainty approximation. The uncertainty is presented in Table 1. Because all presented experimental tests were conducted using the same apparatus, it is understood that the uncertainty does not significantly affect the comparison between the investigated configurations.

TABLE 1: Experimental uncertainty

uncertainty	Unit	h_{is}	ΔP_t
mean	[%]	2.97	1.15
maximum	[%]	8.75	13.5

EXPERIMENTAL RESULTS

Figure 6 presents selected experimental results demonstrating the comparative performance capability of the Tadpole experimental prototypes and normal impinging jets. The 16 mm and 12 mm nozzle throat diameter Tadpole configurations are represented by 16_A and $12_{C,ts}$ respectively while the corresponding impinging jet configurations (Fig. 3, left) are represented by 16_{jet} and 12_{jet}. The flow domain associated with the $12_{C,ts}$ configuration is transonic and is denoted accordingly. An investigation of the impinging jet configurations and their results are presented in [8].

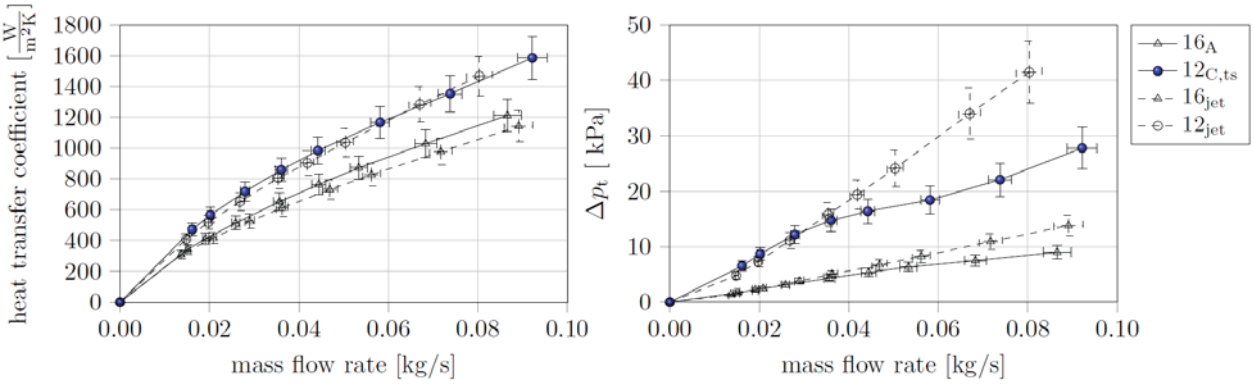

FIGURE 6: A comparison of the overall heat transfer coefficient (left) and the total pressure loss (right) between the experimental results of two Tadpole prototype configurations and the corresponding impinging jet configurations; with the maximum uncertainty shown and the key for both plots is shown on the far right

Impinging jets are known to exhibit good heat transfer capabilities [5]. The experimental results of the impinging jets therefore represents the baseline. The results of 16_A demonstrate that the Tadpole is capable of delivering an enhanced surface heat transfer coefficient while affecting a lower consequential total pressure loss around the domain when compared with the corresponding impinging jet configuration. The $12_{C,ts}$ configuration demonstrates similar heat transfer capabilities with a reduced total pressure loss at higher mass flow rates.

It is concluded that the demonstration of the Tadpole's heat transfer performance shows that it is capable of removing a large heat flux – comparable to or surpassing that of an impinging jet. For this reason, the concept is presented for application in future thermal receivers.

APPLICATIONS OF THE TADPOLE

The Tadpole and its associated design characteristics may be applicable within multiple additional receiver concepts, including the exhibited pyramidal receiver by [3]. The Tadpole may also be capable of improving the performance characteristics of the presented parabolic dish receiver concept in [6]. An implementation of the Tadpole in this dish receiver concept is given in Figure 7 along with a similar cavity structure that has been presented in [2]. The device is called the Tadpole receiver. In this manifestation, the Tadpole exhibits a curved diffuser. The Tadpole is suitable because the heat transfer characteristics within the domain are enhanced at regions where the absorber experiences the peak solar heat flux. In the region where lesser solar flux is experienced, the curved diffuser enables pressure recovery.

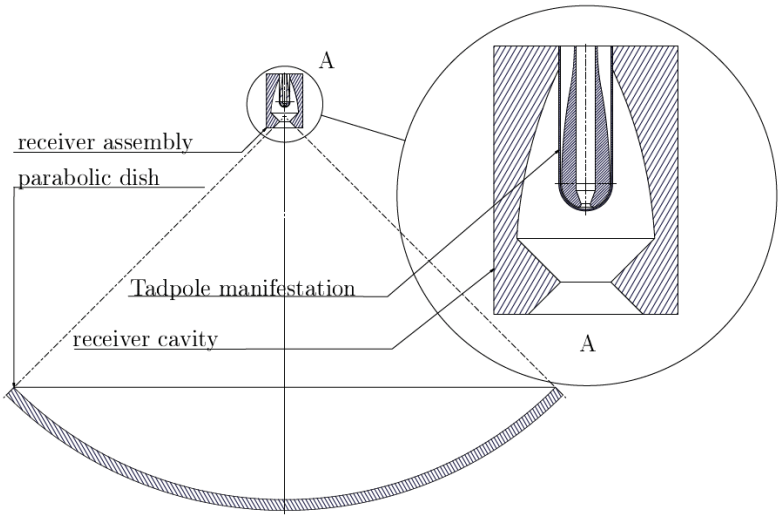

FIGURE 7: The Tadpole receiver: a cross-sectional view of a parabolic dish collector that may improve the performance characteristics of a configuration presented by [6]

The SUNflower receiver is a novel receiver concept and is presented in Figure 8. The SUNflower comprises a hexagonally tessellated array of Tadpole units. The tessellation of the receiver is similar to that of [3] and the cavity structure is similar to one shown in [11]. The device may be capable of absorbing a large solar flux while maintaining a relatively low exterior surface temperature and consequential receiver pressure loss. The three-dimensional absorber structure enables radiation – and re-radiation from neighboring nodes – to be absorbed efficiently.

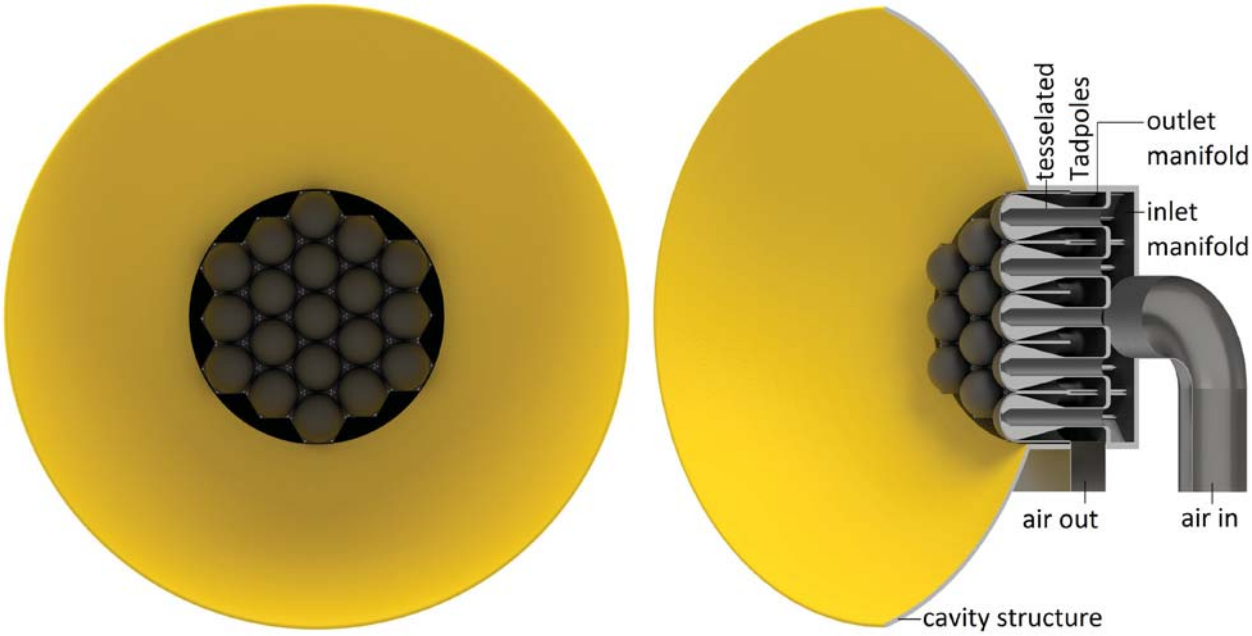

FIGURE 8: The SUNflower: a novel receiver concept

The SUNflower may also be implementable within existing pressurized air receiver concepts such as the SOLHYCO [12] and the SOLUGAS [13]. These receivers both incorporate an array of pipes that are directed toward a rear flat surface as shown in Figure 9.

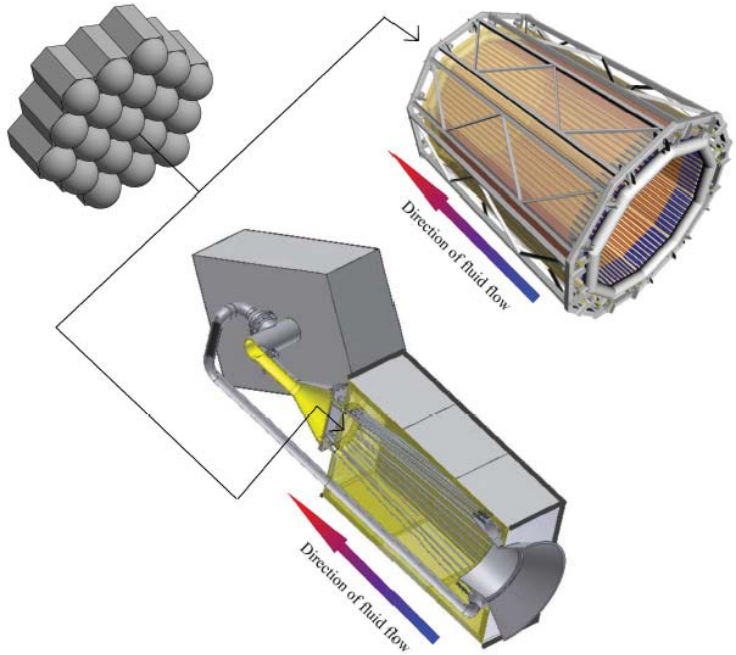

FIGURE 9: A demonstration of two SUNflower applications within existing receiver concepts – SOLUGAS (top) and SOLHYCO (bottom) (adapted from [12 & 13])

The pipe arrays observe the heliostat field with a large incidence angle while the rear surfaces face the heliostat field directly. This region may experience a large solar flux. The SUNflower is envisaged to directly face a heliostat array and can be implemented in this region instead of a reflective coating.

CONCLUSION

A novel impingement heat transfer device has been presented. The performance capabilities of the device were investigated experimentally and compared with impinging jet configurations. The experimental results have shown that the device can outperform an impinging jet. The suitability of the device as a thermal absorber capable of absorbing a concentrated heat flux has been demonstrated. It has further been demonstrated that pressure recovery can improve the performance of an impingement heat transfer device.

The device is applicable within existing receiver concepts. This includes the SCRAP concept and may include the SOLHYCO and SOLUGAS concepts. The device also forms the basis of a novel thermal receiver – the SUNflower.

Further work will focus on predicting the operating performance characteristics of the application concepts.

ACKNOWLEDGMENTS

The authors thank the Solar Thermal Energy Research Group (STERG) and the Centre for Renewable and Sustainable Energy Studies (CRSES) at Stellenbosch University for their support. The assistance and guidance of the Mechanical and Mechatronic Engineering workshop is also greatly appreciated.

REFERENCES

1. R.W. Swindeman and D.L. Marriott (1993). “Criteria for design with structural materials in combined-cycle applications above 815°F”. The American Society of Mechanical Engineers, no. 93-GT-203. Available at: https://doi.org/10.1115/93-GT-203.
2. K.J. Craig, M. Slootweg, J.P. Meyer, J.C. Robbins, R. Kotzé, N.J.M. Honiball, E. Grobler, T.J. Oosthuizen and W. Winterbach (2018). “CFD simulation of solar receiver jet impingement heat transfer: RANS vs LES”. In: 16th International Heat Transfer Conference, vol. 16. Available at: http://hdl.handle.net/10.1615/IHTC16.cms.023262.
3. O. Garbrecht, F. Al-Sibai, R Kneer and K. Wieghardt (2013). “CFD-simulation of a new receiver design for a molten salt solar power tower”. Solar Energy, vol. 90, pp. 94-106. ISSN 0038092X. Available at: http://hdl.handle.net/10.1016/j.solener.2012.12.007.
4. D.G. Kröger (2008). “Spiky Central Receiver Air Pre-heater (SCRAP)”. Tech. Rep., Stellenbosch University.
5. D. McDougall (2018). “Numerical simulation of jet impingement cooling of the inside of a hemisphere with application to SCRAP”. Master's thesis, Stellenbosch University.
6. W. Wang and B. Laumert (2018). “An axial type impinging receiver”. Energy, vol.162, pp. 318 -334. ISSN 0360-5442. Available at: http://hdl.handle.net/10.1016/j.energy.2018.08.036.
7. W. Wang, B. Laumert, H. Xu and T. Strand (2015). “Conjugate heat transfer analysis of an impinging receiver design for a dish-Brayton system”. Solar Energy vol. 119, pp. 298-309 Available at: http://hdl.handle.net/10.1016/j.solener.2015.07.013.
8. D.J. Erasmus, M. Lubkoll, and T.W. Von Backström (2019). “Jet impingement heat transfer within a hemisphere”. ASME journal of heat transfer, under review.
9. M. Lubkoll, T.M. Harms and T.W von Backström (2017). “Introduction to heat transfer test setup for the SCRAP receiver”. In: AIP, vol. 040003, pp. 040003_1 _040003_8. Abu Dhabi. ISBN 9780735415225. Available at: http://hdl.handle.net/10.1063/1.4984399.
10. J. Taylor (1997). “An introduction to error analysis: The study of uncertainties in physical measurement”. 2nd edition. University Science Books, USA.
11. M. Slootweg, K.J. Craig and J.P. Meyer (2019). “A computational approach to simulate the optical and thermal performance of a novel complex geometry solar tower molten salt cavity receiver”. Solar Energy, vol. 187, pp. 13 - 29. ISSN 0038-092X. Available at: https://doi.org/10.1016/j.solener.2019.05.003.
12. L. Amsbeck, R. Buck, P. Heller, J. Jedamski and R. Uhlig (2008). “Development of a tube receiver for a solar hybrid microturbine system”. In: 14th SolarPACES Conference, Las Vegas, NV. Available at: http://www.academia.edu/download/39784364/Development_of_a_tube_receiver_for_a_sol20151107-21591-1xfheo.pdf.
13. R. Korzynietz, J.A. Brioso, A. Del Río, M. Quero, M. Gallas, R. Uhlig, M. Ebert, R. Buck and D. Teraji (2016). “SOLUGAS – Comprehensive analysis of the solar hybrid Brayton plant”. Solar Energy, vol. 135, pp. 578-589. ISSN 0038-092X. Available at: http://hdl.handle.net/10.1016/j.solener.2016.06.020.